Lattice dynamics and migration enthalpies in iron-rich Fe - Al alloys and ordered DO_3 and B2 compounds

1996 J. Phys.: Condens. Matter 8 5535

(http://iopscience.iop.org/0953-8984/8/30/005)

J. Phys.: Condens. Matter **8** (1996) 5535–5553. Printed in the UK

Lattice dynamics and migration enthalpies in iron-rich Fe–Al alloys and ordered DO_3 and B2 compounds

E Kentzinger†, M C Cadeville†, V Pierron-Bohnes†, W Petry‡ and B Hennion§

† IPCMS-GEMM, CNRS, 23 rue du Loess, 67037 Strasbourg, France
‡ Technische Universität München, Physik-Departement E13, James Franck Strasse 1, 85748 Garching, Germany
§ Laboratoire Léon Brillouin, CEN Saclay, 91191 Gif-sur-Yvette, France

Received 16 November 1995, in final form 29 April 1996

Abstract. The phonon dispersion curves of iron-rich Fe–Al alloys have been studied using inelastic neutron scattering. Measurements were performed on three $Fe_{1-x}Al_x$ single crystals at three temperatures, 300 K, 800 K and 1250 K, corresponding to the bcc solid solution for $x = 0.2$ and to three different states of order DO_3, B2 and A2 for $x = 0.25$ and 0.30. The migration enthalpies (H_M) are deduced from the phonon density of states through a model proposed by Schober. They decrease with increasing temperature and have a minimum value at the Fe_3Al composition.

A comparison of the present determination of H_M in Fe–Al with similar H_M-measurements on Fe–Si confirms the contribution of the effective pair interaction energies to the migration enthalpy, as described in models of Monte Carlo simulations of ordering kinetics in B2 and DO_3 compounds.

In the Fe_3Al DO_3 phase, the three separate determinations of H_M (present work), of the formation enthalpy of the vacancies (H_F), and of the activation enthalpy of the ordering kinetics (H_A^{OK}), which are all average quantities, satisfy the addition law: $H_A^{OK} = H_F + H_M$.

1. Introduction

The understanding of the atomic mobility and of related diffusion or ordering kinetics in intermetallic compounds is still a challenge. Jumps to nearest-neighbour (NN) vacancies are nowadays recognized as being the basis for the atom mobility in cubic metals (Peterson 1978, Ait Salem *et al* 1979, Göltz *et al* 1980, Herzig 1983, Vogl *et al* 1989, Petry *et al* 1991) in which both the concentration of vacancies and their migration enthalpies are important quantities that drive the mobility. Experimental methods like radiotracer diffusion or ordering kinetics basically yield macroscopic transport coefficients. Two thermodynamic quantities are deduced from the Arrhenius plots of the diffusion coefficient D or of the relaxation time τ of ordering: (i) the pre-exponential factors D_0 or τ_0; and (ii) the activation enthalpy (H_A) of each process. In intermetallic compounds having non-equivalent sublattices, the activation enthalpy results from many contributions that are at least: (i) the formation enthalpies of vacancies (H_F) on each sublattice; and (ii) the migration enthalpies (H_M) depending on which of the species is migrating and of their initial and final sublattices. In order to get a clearer insight into all of these quantities, experiments that yield separate information either on the formation enthalpy of vacancies, or on their migration enthalpy

0953-8984/96/305535+19$19.50

must be considered. It is the purpose of the present work to focus on the determination of migration enthalpies in iron-rich Fe–Al alloys and ordered compounds.

A lot is already known on the diffusion properties in these alloys. Whereas radiotracer diffusion experiments on Al or Fe in Fe_3Al yield high activation enthalpies of respectively 2.76 and 2.6 eV (Larikov *et al* 1981), i.e. of the same order of magnitude as the self-diffusivity in pure iron (2.6 eV in the paramagnetic range (Lubbehusen and Mehrer 1990)), an important decrease of the activation enthalpy with Al content ($H_A = 1.78$ eV for $x = 0.18$) in the solid-solution phase was reported by Raghunathan and Sharma (1981) from a ^{59}Fe tracer diffusion experiment. More recently, Tökei *et al* (1996) have measured the self-diffusion coefficient of ^{59}Fe in Fe_3Al in the solid-solution phase ($H_A^D = 2.12$ eV) and in the B2 phase. They observe a downward curvature of the Arrhenius plot that is assigned to the B2 type of atomic order. Vennéguès *et al* (1990) found, in experiments probing the kinetics of ordering, a strong decrease of the activation enthalpy with increasing Al content, leading to a small H_A-value of 1.4 ± 0.2 eV around the Fe_3Al composition in the DO_3 phase. Besides this, the vacancy concentration was determined in Fe_3Al from positron annihilation experiments by Schaefer *et al* (1990) as a function of temperature, giving a formation enthalpy H_F of vacancies of 1.18 ± 0.04 eV, a value that is small compared to the value of 1.8 eV for pure iron given by Schultz (1991). Assuming first, in a very crude approximation, that for Fe_3Al the activation energy is the sum of its formation and migration counterparts independently of considerations of an eventual temperature dependence, the values of the migration enthalpy H_M that we deduce from diffusion in the A2 phase (Tökei *et al* 1996) or ordering kinetics in the DO_3 phase seem to be very different, being either very high ($\sim$0.9 eV from diffusion) or very low ($\sim$0.2 eV from ordering kinetics). In order to solve or to understand this apparent contradiction, a direct determination of the migration enthalpy and of its temperature dependence is necessary.

There are several experimental approaches for determining the migration enthalpy directly. Its direct determination in pure metals or alloys can be obtained for example from the temperature of the stage III resistivity annealing after low-temperature irradiation, as described by Schultz (1991). Another method is that based on short-range ordering kinetics through resistometry (Balanzat and Hillairet 1981, Afyouni *et al* 1989) that yields simultaneously H_F, H_M and H_A. This last method requiring very highly homogeneous samples rests on the hypothesis that all of these quantities are temperature independent.

Recently a model relating the migration enthalpy for NN vacancy jumps in cubic metals to the phonon dispersion has been proposed by Schober *et al* (1992). It was applied first to fcc and bcc metals (Schober *et al* 1992, Güthoff *et al* 1994). In pure fcc metals an excellent agreement between the calculated and measured values of H_M was found, whereas in bcc metals, where the experimental values are less well known, predictions were obtained that show a pronounced chemical group systematic. More recently, the same *ansatz* has been used by Randl *et al* (Randl 1994, Randl *et al* 1995) to estimate the migration barriers in $Fe_{1-x}Si_x$ ($x = 0.20$, 0.25) alloys, an intermetallic system with a phase diagram very similar to that of Fe_3Al (Köster and Gödecke 1980). Strictly speaking, the *ansatz* for H_M is only valid for monatomic structures, because it assumes that diffusion takes place via nearest-neighbour jumps only. In general this cannot be assumed for intermetallics. However, for both Fe_3Si (Sepiol and Vogl 1993) and $Fe_{0.66}Al_{0.33}$ (Feldwisch *et al* 1995), quasielastic Mössbauer spectroscopy has shown that the elementary diffusion jump essentially is a jump to the nearest-neighbour site. Therefore, as a first approximation, we consider the DO_3 as well as the B2 structure as a bcc lattice with atoms of a mass corresponding to the average mass of the alloy.

The prerequisite for such an evaluation of H_M is the precise knowledge of the phonon

dispersion for the different states of order, where order is a function of both composition and annealing temperature. For the stoichiometric compound Fe_3Al phonon dispersion curves have already been measured in great detail. Van Dijk (1970) obtained an almost complete set of results at room temperature (RT) for DO_3-ordered Fe_3Al but did not examine the other states of order. Robertson (1991) has investigated at RT the different states of order of quenched alloys, but he has measured phonon frequencies only below 9 THz. In the present paper we report for the first time an investigation of the total phonon frequencies in iron-rich $Fe_{1-x}Al_x$ alloys as a function of the concentration ($x = 0.20$, 0.25 and 0.30) and the temperature (300 K, 800 K, 1250 K) for several states of order (A2-disordered bcc, DO_3- and B2-ordered structures).

This paper is organized as follows. In section 2 we recall some features of the phase diagram and the ordered structures of the iron-rich Fe–Al system. The experimental procedure is described in section 3. Section 4 is devoted to results of phonon dispersion measurements, to their qualitative discussion, to their simulation using a Born–von Kàrmàn (BvK) model in the axial approximation and to the calculation of the phonon density of states. In section 5 the migration enthalpies are deduced from the density of states, and discussed comparatively with determinations of H_M by other methods. Section 6 is a general discussion of the data, comparing with similar results for Fe–Si DO_3 compounds and with diffusion and ordering kinetics data for around the Fe_3Al composition. Conclusions are drawn in section 7.

2. Some established results

The iron-rich side of the Fe–Al phase diagram as determined by Köster and Gödecke (1980) and confirmed by Afyouni (1989) is shown in figure 1. It displays the A2 solid-solution phase and the DO_3- and B2-ordered structures, depending on concentration and temperature. The ferro–paramagnetic transition line is also represented showing the disappearance of the long-range ferromagnetic order at around 30 at.% of Al. The DO_3 structure consists of four interpenetrating fcc sublattices with two of them (α and δ) being equivalent. In the case of ideal ordering the Al atoms occupy only the β-sublattice. More generally, the long-range-order (LRO) state is determined by two LRO parameters: if $\langle P_{Al}^i \rangle$ is the probability of occupation of the sublattice i by an Al atom, one has

$$\begin{aligned} \eta_1 &= \frac{1}{2}[\langle P_{Al}^{\beta} \rangle - \langle P_{Al}^{\gamma} \rangle] \\ \eta_2 &= \frac{1}{2}[\langle P_{Al}^{\beta} \rangle + \langle P_{Al}^{\gamma} \rangle - 2\langle P_{Al}^{\alpha,\delta} \rangle]. \end{aligned} \tag{1}$$

In the B2 structure, the sublattices β and γ are equivalent ($\eta_1 = 0$), i.e. the Al atoms occupy the β- and γ-sublattices with equal probability, and one has a single order parameter:

$$\eta = \eta_2 = \langle P_{Al}^{\beta,\gamma} \rangle - \langle P_{Al}^{\alpha,\delta} \rangle. \tag{2}$$

The structures of DO_3 and B2 are shown in the insets of figure 1.

According to the phase diagram of figure 1, $Fe_{80}Al_{20}$ has the disordered A2 structure at high temperature and is two-phase A2 + DO_3 below about 650 K. However, due to the very sluggish character of the A2 $\rightarrow$ A2 + DO_3 phase decomposition, it is very easy to quench the disordered A2 structure to room temperature. When correctly annealed, $Fe_{75}Al_{25}$ and $Fe_{70}Al_{30}$ display at increasing temperature successively the DO_3, B2 and A2 structures. Figure 2(a) displays the temperature dependence of the two order parameters η_1 and η_2 for $Fe_{75}Al_{25}$ calculated by Sanchez (1995) using the same model as used by

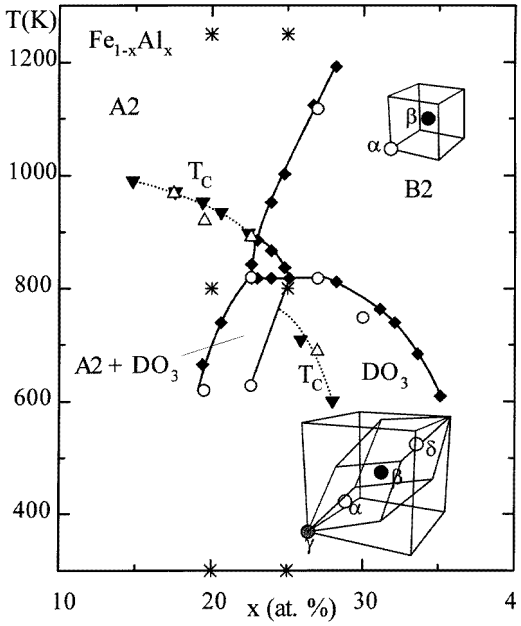

Figure 1. The iron-rich part of the Fe–Al phase diagram from Köster and Gödecke (1980) (⧫, ▼) and Afyouni (1989) (○, △). The dotted line shows the magnetic transition temperatures. The stars indicate the measurement temperatures. The Bravais lattices and the primitive unit cells of the two ordered structures B2 and DO_3 are in the insets.

Cadeville *et al* (1992) for $Fe_{70}Al_{30}$. Due to the lack of diffusion at low temperatures, the maximum values of η_1 are never reached. The LRO parameter values at the temperatures where the phonon spectra were measured are deduced from the calculated values shown in figure 2(*a*), taking into account the ordering kinetics data of Vennéguès *et al* (1990), as given hereafter in section 3.2.

Finally, figure 2(*b*) shows a $(1\bar{1}0)$ cut through reciprocal space including the Brillouin zones for the different states of order.

3. Experimental procedure

3.1. Sample preparation

The preparation of the $Fe_{80}Al_{20}$ single crystal has been reported by Pierron-Bohnes *et al* (1990). The sample was a cylinder 20 mm long and 10 mm in diameter. The composition was checked through various techniques; the aluminium concentration was 19.5 ± 0.3 at.% Al. The composition fluctuations on the slice surface were within 0.3%. The mosaicity of the crystal was measured through γ-ray diffraction (Pierron-Bohnes *et al* 1989) and was 0.5. The $Fe_{70}Al_{30}$ single crystal was provided by Metals Crystals and Oxides Ltd, Cambridge, UK. The sample was a cylinder 9 mm long and 9 mm in diameter. The quality of the crystal was checked during the neutron scattering experiment. From the width of several Bragg peaks on different scattering planes the mosaicity has been estimated to be 0.6. After a first set of phonon dispersion measurements, this crystal was transformed accidentally to $Fe_{75.2}Al_{24.8}$ by partial sublimation during a neutron diffuse scattering experiment to measure

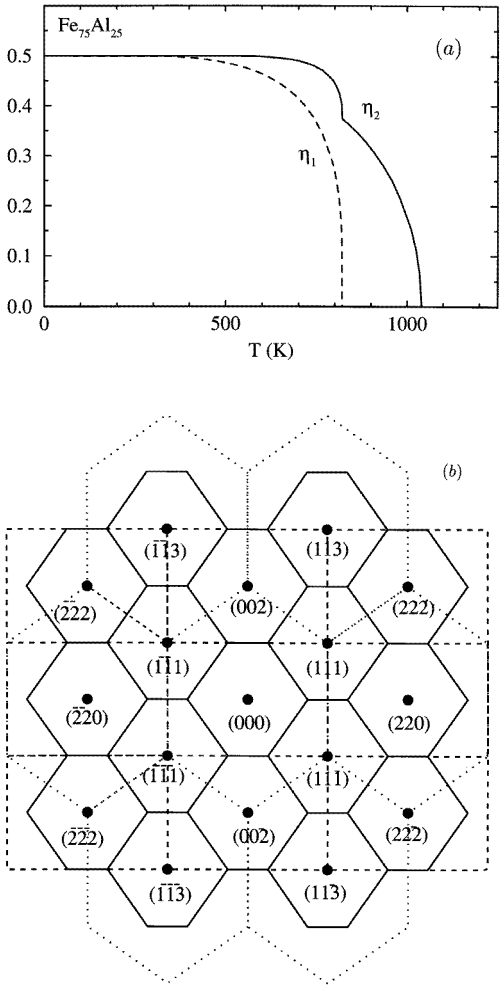

Figure 2. (*a*) Calculated LRO parameters for the $Fe_{75}Al_{25}$ compound as a function of temperature according to Sanchez (1995); see the text for further details. (*b*) Brillouin zone boundaries in the $(1\bar{1}0)$ plane of the reciprocal space. The dotted lines are the bcc boundaries, the dashed lines the B2 boundaries and the solid lines are the DO_3 boundaries. The Miller indices refer to the DO_3 structure.

the short-range order. This experiment was performed at 1100 °C for several days. Its final concentration and homogeneity were checked by chemical analysis and scanning electron microscopy, giving an absolute uncertainty on the Al concentration of 1.0 at%. A set of phonon measurements were performed again on this single crystal.

3.2. Heat treatments

The annealing times to get samples in thermodynamically ordered states were chosen in agreement with the results on ordering kinetics measured by Vennéguès *et al* (1990). They were set to be at least 10 times the relaxation times for ordering. During the heat treatments,

the samples were wrapped in a tantalum foil to prevent them from oxidation and sealed in a quartz container under 10^{-6} Torr residual pressure. The $Fe_{80}Al_{20}$ sample was heated for 1 h at 1075 K and 16 h at 875 K for homogenization, then 1 h at 825 K, 2 h at 775 K, and quenched in ice water in order to keep the solid-solution phase down to 300 K.

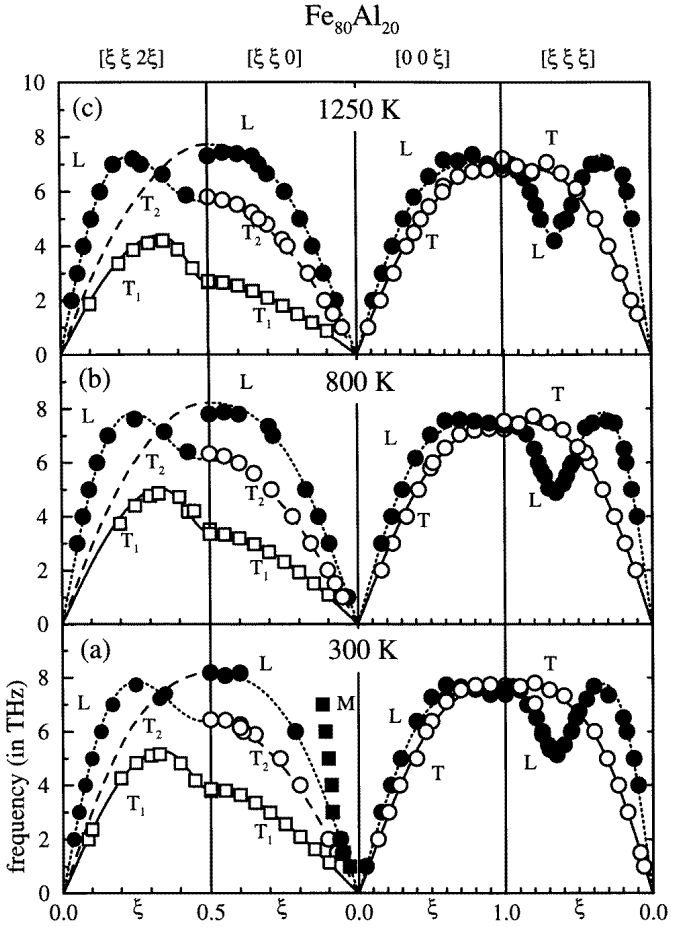

Figure 3. Phonon dispersion curves measured for $Fe_{80}Al_{20}$ at three temperatures: 300 K (*a*), 800 K (*b*) and 1250 K (*c*). ξ is the reduced wave vector in bcc units. The filled squares at 300 K indicate measured magnons. The lines correspond to BvK fits as described in the text.

To 'catch' the DO_3 phase, the $Fe_{75}Al_{25}$ sample was heated for 21 h at 1075 K and quenched in ice water. Then it was heated for 44 h at 875 K and quenched in ice water to avoid the critical slowing down at the B2–DO_3 order–order transition. It was then annealed in the DO_3 region: 92 h at 725 K, 212 h at 675 K, 117 h at 625 K, 390 h at 575 K, and then quenched in ice water to retain the ordered state at 575 K. Below this temperature the annealing times increase considerably without any appreciable increase of the LRO. The same heat treatment, with approximately the same annealing times, was performed on the $Fe_{70}Al_{30}$ sample.

3.3. Neutron inelastic scattering experiments

The neutron inelastic scattering experiments were performed on the triple-axis spectrometer 1T at the Laboratoire Léon Brillouin (LLB). In most cases the final wave vector was fixed at $k_f = 2.662$ Å^{-1} and scans were performed either in the constant-($h\nu$) mode or in the constant-$\boldsymbol{Q}$ mode, depending on the slope of the phonon dispersion at the measured ($\boldsymbol{q}$, ν) point. Typical energy resolutions at zero energy transfer of 0.25 THz have been measured. Most of the phonons have been measured in the (110) plane. However, to have access to the transverse $T_{[1\bar{1}0]}[\xi\xi 0]$ dispersions, the (100) plane has been set parallel to the scattering plane. Adequate Brillouin zones have been chosen in order to measure the different phonon branches at their structure factor maximum.

Measurements were set up at the three temperatures 300, 800 and 1250 K. The high temperatures were achieved by means of a standard ILL (Institut Laue–Langevin) resistance furnace. The vacuum was of the order of 10^{-6} Torr. The sample temperature was monitored with two independent thermocouples. The uncertainty is of the order of 10 K.

According to the heat treatments and the phase diagram, the three measuring temperatures correspond, respectively: in $Fe_{80}Al_{20}$ to the A2 solid-solution phase, short-range ordered at 775, 800 and 1250 K; in $Fe_{75}Al_{25}$ to the DO_3 phase long-range ordered at 575 and 800 K (see figure 2(*a*) for the values of the LRO parameters) and to the A2 solid-solution phase at 1250 K; in $Fe_{70}Al_{30}$ to the DO_3 phase long-range ordered at 575 K, to the B2 phase long-range ordered at 800 K (see Cadeville *et al* (1992) for the values of the LRO parameters) and to the A2 solid-solution phase short-range ordered at 1250 K.

The temperature of 800 K had been initially chosen to measure the $Fe_{70}Al_{30}$ in the most ordered state of the B2 structure. For $Fe_{75}Al_{25}$, this temperature corresponds to the superior limit of the existence of the DO_3 phase, i.e. it is very close to the DO_3–B2 transition. At 800 K the LRO parameter η_1 which characterizes the DO_3 structure is far from its maximum value, whereas the LRO parameter η_2 which characterizes the B2 order is close to its maximum value (see figure 2(*a*)). For this reason and considering the uncertainty in the determination of the furnace temperature, the dispersion curves at 800 K were set up and fitted in the B2 structure. As we shall see later in this paper, this procedure has a negligible effect on the determination of the migration enthalpy at this temperature.

4. Results

4.1. Phonon branches

The measured frequencies $\nu(\boldsymbol{q})$ of the phonon dispersion are reported in figures 3 and 4. For the ordered alloys, we use the same notation as Randl (1994) to recall the irreducible representations of the point group that they belong to.

As a general trend, one observes an overall decrease of the low-energy branches (frequencies lower than 9 THz) with increasing temperature and Al concentration. The $Fe_{80}Al_{20}$ sample, which conserves the disordered bcc structure over the whole explored T-range, displays the specific features of phonon dispersions in a bcc lattice: (i) a pronounced dip in the vicinity of the longitudinal $\frac{2}{3}$[111] branch; and (ii) low frequencies of the transverse $[\xi\xi 0]$ branch with $[1\bar{1}0]$ polarization ($T_1[\xi\xi 0]$). Both features are generic to the open geometry of the bcc lattice (Petry 1995). The decrease of all phonon frequencies with increasing temperature indicates a softening of the lattice as the temperature is increased. In the $Fe_{75}Al_{25}$ when going from the disordered phase to the ordered B2 and DO_3 structures, new branches appear due to the increase of the number of atoms per unit cell. A striking

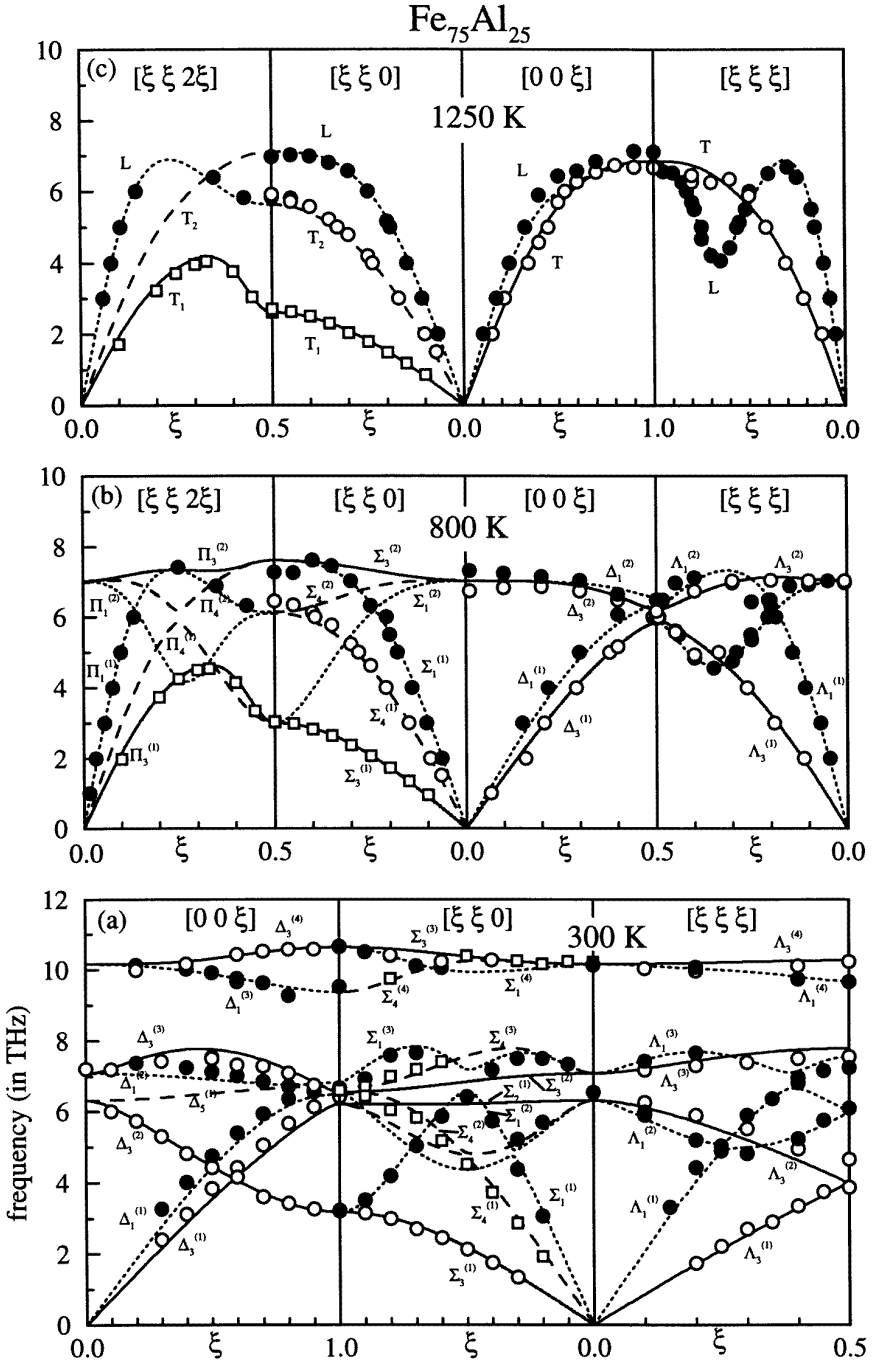

Figure 4. Phonon dispersion curves measured for $Fe_{75}Al_{25}$ at three temperatures. ξ is the reduced wave vector in bcc units except in (*a*) (DO_3 units). The lines correspond to BvK fits as described in the text.

effect is the appearance of high-frequency optical modes in the DO_3 structure which are clearly separated from the lower optical and acoustic branches. Branches that belong to the same irreducible representation of the point group do not cross each other. But, in the case of our system, the induced gaps remain very small and have not been observed within the experimental resolution. This will be reflected in the calculated density of states where below 8 THz no gaps are visible. In the related system Fe_3Si (Randl *et al* 1995) this splitting is more pronounced and its collapse has been used as an indication of increasing disorder. Phonon branches below 9 THz have also been measured in $Fe_{70}Al_{30}$ but, due to the incompleteness of the measurement, we do not show them here.

The dispersion curves of the $Fe_{75}Al_{25}$ alloy at room temperature can also be compared to those measured by Van Dijk (1970) for the stoichiometric Fe_3Al compound. We do not see any big difference in the acoustic modes and in the first optical modes. The optical modes around 10 THz are slightly higher in the Fe_3Al case of Van Dijk's data by about 0.5 THz.

4.2. Born–von Kàrmàn fits

The measured frequencies $\nu(\boldsymbol{q})$ have been fitted using the harmonic approximation and a Born–von Kàrmàn model. In the harmonic approximation, the equation of motion of the displacement $\boldsymbol{u}(l\lambda)$ of atom λ in the unit cell l from its equilibrium position is

$$M_\lambda \frac{\mathrm{d}^2\boldsymbol{u}(l\lambda)}{\mathrm{d}t^2} = -\sum_{l'\lambda'} \Phi(l\lambda; l'\lambda')\boldsymbol{u}(l'\lambda') \tag{3}$$

where M_λ is the mass of atom λ and $\Phi(l\lambda; l'\lambda')$ is the 3×3 matrix of second derivatives at the equilibrium state of the crystal potential energy with respect to the three components of $\boldsymbol{u}(l\lambda)$ and $\boldsymbol{u}(l'\lambda')$.

We use the axially symmetrical force constant model first developed by Lehman *et al* (1962), i.e. we assume the matrix $\Phi(l\lambda; l'\lambda')$ to be of the form

$$\Phi(l\lambda; l'\lambda') = (T_n(\lambda\lambda') - L_n(\lambda\lambda'))\begin{pmatrix} r_x^2 & r_x r_y & r_x r_z \\ r_x r_y & r_y^2 & r_y r_z \\ r_x r_z & r_y r_z & r_z^2 \end{pmatrix} - T_n(\lambda\lambda')\begin{pmatrix} 1 & 0 & 0 \\ 0 & 1 & 0 \\ 0 & 0 & 1 \end{pmatrix} \tag{4}$$

where

$$(r_x, r_y, r_z) = \frac{\boldsymbol{r}(l'\lambda') - \boldsymbol{r}(l\lambda)}{|\boldsymbol{r}(l'\lambda') - \boldsymbol{r}(l\lambda)|}.$$

$\boldsymbol{r}(l\lambda)$ is the equilibrium position of atom λ in the unit cell l. The $L_n(\lambda\lambda')$ are called longitudinal and the $T_n(\lambda\lambda')$ transversal force constants of the nth nearest-neighbour interaction between atoms λ and λ'. Usually, the transversal force constants are about one order of magnitude lower than the longitudinal ones.

This force constant model has been used to fit the measured points. It assumes that the potential energy of the crystal is a sum of spherical two-body potentials taken over all pairs $(l\lambda, l'\lambda')$ of lattice sites. The interaction between any two atoms at any distance from each other is reduced to two force constants. This reduction to axially symmetrical forces instead of using the more generalized force tensor model greatly simplifies the interpretation of the force constants. The number of neighbouring shells that we took into account was increased until the fit quality did not vary any more. Interactions up to the fifth neighbours have been taken into account for fits in the bcc solid-phase solution, which corresponds to 10 parameters. In the B2 and DO_3 phases, respectively 16 and 14 parameters were needed.

Table 1. Interatomic force constants (in N m^{-1}) for $Fe_{75}Al_{25}$ and for $Fe_{80}Al_{20}$.

DO_3	$Fe_{75}Al_{25}$		$Fe_{75}Al_{25}$		$Fe_{80}Al_{20}$	$Fe_{80}Al_{20}$	$Fe_{80}Al_{20}$	$Fe_{75}Al_{25}$
T (K)	300	B2	800	A2	300	800	1250	1250
$L_1(\alpha\gamma)$	42.9(6)	$L_1(\alpha\beta)$	29.3(4)	L_1	34.3(7)	34.7(7)	31.3(5)	26.5(5)
$T_1(\alpha\gamma)$	0.3(1)	$T_1(\alpha\beta)$	−0.5(2)	T_1	1.0(3)	−0.6(3)	−1.2(2)	−0.6(2)
$L_1(\alpha\beta)$	53.5(6)	$L_2(\alpha\alpha)$	3.3(8)	L_2	5.6(7)	7.4(7)	5.8(5)	1.5(5)
$T_1(\alpha\beta)$	−1.4(1)	$T_2(\alpha\alpha)$	2.2(2)	T_2	1.4(3)	0.9(4)	0.2(3)	0.7(2)
$L_2(\beta\gamma)$	11.7(6)	$L_2(\beta\beta)$	0.4(1)	L_3	3.4(3)	3.6(3)	3.3(3)	2.7(2)
$T_2(\beta\gamma)$	−2.1(3)	$T_2(\beta\beta)$	0.9(2)	T_3	−0.3(2)	−0.9(2)	−0.9(2)	−0.3(2)
$L_3(\alpha\delta)$	3.1(5)	$L_3(\alpha\alpha)$	5.4(4)	L_4	0.5(2)	0.6(2)	0.4(2)	1.0(1)
$T_2(\alpha\delta)$	0.9(1)	$T_3(\alpha\alpha)$	−0.2(1)	T_4	−0.3(1)	−0.1(1)	0.2(1)	−0.2(1)
$L_3(\gamma\gamma)$	4.3(2)	$L_3(\beta\beta)$	2.1(2)	L_5	2.5(4)	1.3(4)	1.5(3)	2.3(3)
$T_3(\gamma\gamma)$	−0.2(1)	$T_3(\beta\beta)$	0.0(0)	T_5	0.2(2)	0.2(1)	0.0(0)	0.1(1)
$L_3(\alpha\alpha)$	4.5(3)	$L_4(\alpha\beta)$	0.7(1)					
$T_3(\alpha\alpha)$	−0.6(1)	$T_4(\alpha\beta)$	−0.2(1)					
$L_3(\beta\beta)$	0.3(1)	$L_5(\alpha\alpha)$	3.5(2)					
$T_3(\beta\beta)$	0.1(1)	$T_5(\alpha\alpha)$	0.0(0)					
		$L_5(\beta\beta)$	3.0(2)					
		$T_5(\beta\beta)$	0.0(0)					

Fits in the bcc solid solution were performed using the average mass of the alloy. For the fits in the two ordered structures, we used the average mass per site, taking into account the occupation numbers deduced from the order parameters given in section 2. The results of such fits are the lines in figures 3 and 4. The resulting force constants are given in table 1. For those fits, we assumed that the relative error on all frequencies was 3%, which is a good mean estimate.

4.3. Total and weighted densities of states

Using the atomic force constants obtained, we calculated the normalized phonon density of states (DOS) at each temperature and concentration. It is obtained from the dispersion relations $\nu_j(\boldsymbol{q})$ by an integration over the first Brillouin zone:

$$Z(\nu) = \frac{V}{(2\pi)^3} \sum_j \int \delta(\nu - \nu_j(\boldsymbol{q}))\ \mathrm{d}\boldsymbol{q} \tag{5}$$

where V is the volume of the unit cell.

The calculated densities of states for the three temperatures and two compositions are shown in figure 5. Nothing else can be added to the above discussion on the dispersion relations: we clearly see here the general shift of the spectrum to the lower frequencies when the Al concentration and temperature are increased.

Another interesting quantity is the so-called weighted phonon DOS for the atom λ:

$$Z_\lambda(\nu) = \frac{V}{(2\pi)^3} \sum_j \int |\boldsymbol{e}_\lambda^j(\boldsymbol{q})|^2 \delta(\nu - \nu_j(\boldsymbol{q}))\ \mathrm{d}\boldsymbol{q} \tag{6}$$

where $\boldsymbol{e}_\lambda^j(\boldsymbol{q})$ is the normalized eigenvector at the wave vector $\boldsymbol{q}$ of the dynamical matrix for the basis atom λ in the unit cell and for the phonon branch j. The sum of the different weighted DOS corresponding to the different sites in the unit cell gives the DOS. In the DO_3 structure, we have three non-equivalent lattice sites in the unit cell leading to three non-equivalent weighted DOS.

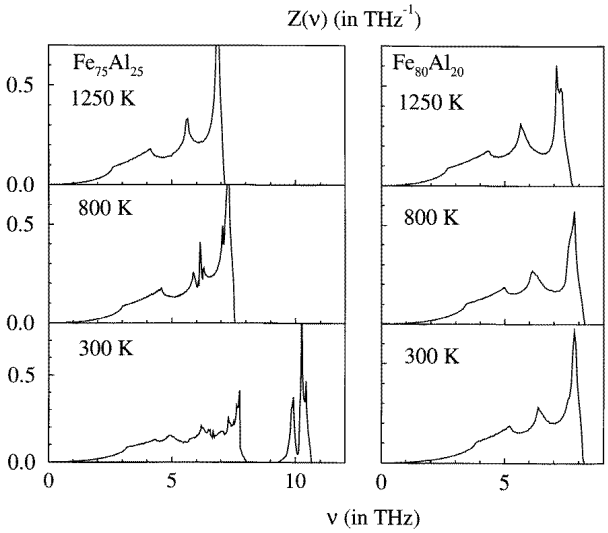

Figure 5. Normalized phonon densities of states (in THz^{-1}) for $Fe_{75}Al_{25}$ and $Fe_{80}Al_{20}$ at the temperatures studied.

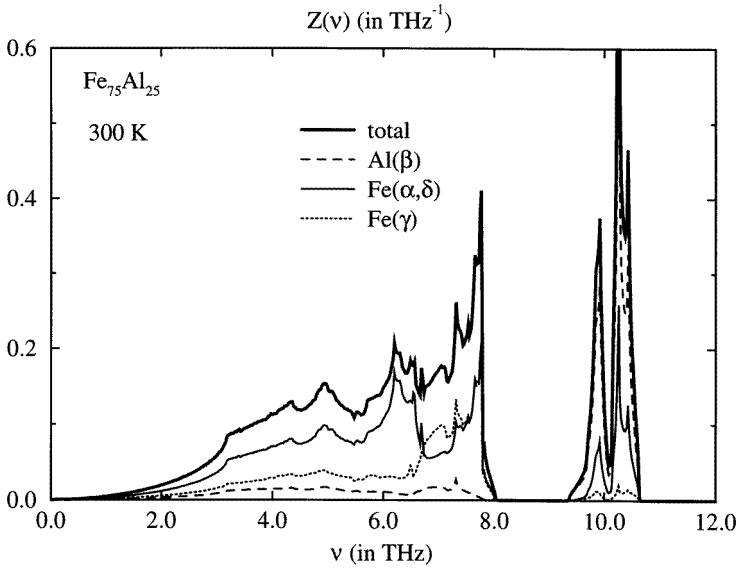

Figure 6. Total and weighted densities of states at 300 K for $Fe_{75}Al_{25}$, as calculated from the BvK force constants.

In figure 6 we give, with the total DOS, the three calculated weighted DOS for our $Fe_{75}Al_{25}$ compound at 300 K. We can see from this figure that the contribution from the β-sites, occupied by Al atoms, to the total frequency distribution arises mainly from the high-energy optical modes while the contribution from the γ-sites, occupied by Fe atoms and surrounded only by Fe atoms as first neighbours, arises from modes of frequencies

lower than 8 THz. The modes of the α- and δ-sites, which have four Al and four Fe as nearest neighbours, are distributed between low and high frequencies.

5. The migration enthalpies

Several thermodynamical quantities can be deduced from the phonon DOS obtained: they are the migration enthalpy H_M, the vibrational entropy, the lattice specific heat, and the mean square displacements and the related Debye temperature. In this paper, we focus our interest on the determination of the migration enthalpies, the other quantities being discussed by Kentzinger (1996).

As mentioned in the introduction, the model recently developed by Schober *et al* (1992) to deduce the migration enthalpy from the phonon dispersion was first applied successfully to pure cubic fcc and bcc metals and more recently to intermetallics Fe_3Si and Ni_3Sb (Randl 1994, Randl *et al* 1995). For Fe_3Al it provides us with the possibility of estimating H_M; no direct measurements of H_M exist.

In this model, the migration enthalpy is based on the following relation:

$$H_M = 4\pi^2 a^2 \alpha G_0^{-1} \tag{7}$$

where

$$G_0 = \int \frac{Z(\nu)}{M\nu^2}\,\mathrm{d}\nu.$$

In (7), H_M separates into a structural term (αa^2) common to all bcc and derived DO_3 and B2 structures, and a term (G_0) which is the static Green function that reflects the peculiarities of the metal or alloy investigated. a is the lattice parameter, $\alpha_{bcc} = 0.0130(7)$ is a geometrical constant that has been determined by computer simulations and M is the average mass of the alloy. Being aware that this model has been developed for pure metals, we have used it to estimate the average migration enthalpy. Let us recall that the specific part of the displacement potential is introduced by the minus-second moment of $Z(\nu)$, i.e. the static Green function G_0. It is due to the weighting by ν^{-2} that low-energy phonons are the essential quantities for probing the migration barrier.

The Schober model builds on the earlier ideas of Flynn (1968), who related H_M to the elastic constants, according to the following relation:

$$H_M^V = C\Omega\delta^2 \tag{8}$$

where

$$\frac{15}{12C} = \frac{3}{C_{11}} + \frac{2}{(C_{11} - C_{12})} + \frac{1}{C_{44}}.$$

C_{11}, C_{12}, C_{44} are the three independent elastic constants of the material, and Ω is the atomic volume. $\delta = q/s$ is a dimensionless constant that reflects the ratio of a hypothetical cut-off distance q of the harmonic potential towards the saddle-point distance s: like Schober *et al* (1992), we took $\delta^2 = 0.041$ for bcc metals and derived ordered structures. This value has been adjusted in order to reproduce $H_M = 1.7$ eV for W, a metal that is representative of what is called normal self-diffusivity. The C_{ij} are related to the sound velocities $v_{T1,}v_{T2}$ and v_L in the [110] direction, giving

$$\begin{aligned} C' &= \frac{1}{2}(C_{11} - C_{12}) = \rho v_{T_1}^2 \\ C_{44} &= \rho v_{T_2}^2 \\ C_L &= \frac{1}{2}(C_{11} - C_{12} + 2C_{44}) = \rho v_L^2. \end{aligned} \tag{9}$$

Those velocities can be obtained either by ultrasonic measurements or from the slopes at the origin ($\xi = 0$) of the phonon dispersion curves. Leamy *et al* (1967) have determined C_{ij} from ultrasonic measurements between 77 K and 300 K and for 12 Al concentrations between 0 and 40 at.%.

Table 2. Migration enthalpies (in eV) calculated in the Schober model and in the Flynn model for $Fe_{1-x}Al_x$, pure Fe (Schober *et al* 1992) and $Fe_{1-x}Si_x$ as given by Randl *et al* (1995).

Alloy	T (K)	H_M(Sch)	H_M(Fly)
Fe	300	0.66(6)	0.57(4)
$Fe_{80}Al_{20}$	300	0.55(6)	0.45
	800	0.50(6)	0.42(4)
	1250	0.41(6)	0.30(4)
$Fe_{75}Al_{25}$	300	0.52(6)	0.37(4)
	800	0.46(6)	0.35(4)
	1250	0.39(6)	0.29(4)
$Fe_{70}Al_{30}$	300		0.42(4)
$Fe_{80}Si_{20}$	300	0.60(3)	
$Fe_{75}Si_{25}$	300	0.59(3)	

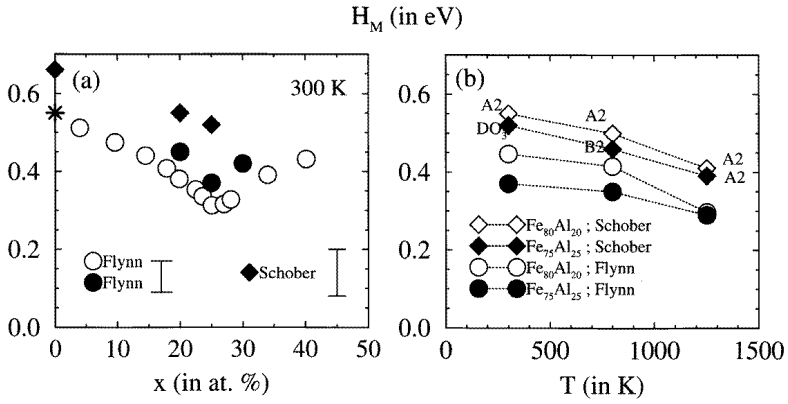

Figure 7. (*a*) Migration enthalpies (in eV) at 300 K for $Fe_{1-x}Al_x$ calculated in the Schober model (♦) and in the Flynn model from elastic constants measured by Leamy *et al* (1967) (○) and from the initial slopes of our phonon dispersion curves (●). The star at $x = 0$ is the experimental value given by Schultz (1991). For each model a typical error bar is shown in the picture. (*b*) Evolution of the migration enthalpies as a function of temperature for $Fe_{80}Al_{20}$ (empty symbols) and for $Fe_{75}Al_{25}$ (filled symbols) in the Schober model (diamonds) and in the Flynn model (circles). Dotted lines are guides for the eyes. The uncertainties are the same as in figure 7(*a*).

The values of H_M are calculated in the Schober model for $x = 0.20$ and 0.25 at three temperatures (300, 800 and 1250 K) and in the Flynn model using either our measurements for $x = 0.20$, 0.25 and 0.30 or the data of Leamy at 300 K. These values are gathered together in table 2 and compared with similar data for pure Fe and for the Fe–Si system (Randl *et al* 1995). Figures 7(*a*) and 7(*b*) display the evolution of H_M with Al concentration and temperature.

5.1. The evolution of H_M with the Al concentration

The concentration dependence at 300 K of H_M in the Schober model (H_M(Sch)) is shown by the diamonds in figure 7(*a*). The value for pure iron (0.66 eV) is that determined by Schober *et al* (1992) for the same model. One observes a clear decrease of H_M with x.

The values of H_M in the Flynn model (H_M(Fly)) are the circles in figure 7(*a*): empty circles correspond to the elastic constants determined by Leamy, and filled circles correspond to those deduced from our measurements. The experimental determination of H_M in pure iron (0.55 eV given by Schultz (1991); the star in figure 7(*a*)) is in quite good agreement with the limit value of H_M(Fly) at $x = 0$. Within each set of data we see an important decrease of H_M(Fly) of about a factor 2 from pure iron to Fe_3Al, followed by an increase beyond the stoichiometry. We then obtain a minimum of H_M(Fly) at the DO_3 stoichiometry.

Partial measurement of the dispersion curves below 9 THz for $Fe_{70}Al_{30}$ yields a value of H_M(Sch) equal to 0.50 eV that can be compared to the equivalent determination (below 9 THz) in $Fe_{75}Al_{25}$ which is 0.41 eV, thus confirming the existence of a minimum of H_M at the DO_3 stoichiometry.

The values of H_M(Sch) are clearly higher than those of H_M(Fly) at any concentration, a trend that is opposite to that observed in bcc transition metals, in which H_M(Fly) is higher than H_M(Sch) by about 0.15 eV, other than for Fe. Nevertheless, a clear result of our investigation at 300 K is the low value of H_M in these Fe–Al alloys and the presence of a minimum at the DO_3 stoichiometry.

5.2. Evolution of H_M with temperature

Figure 7(*b*) represents the temperature dependence of H_M in the two models for $Fe_{80}Al_{20}$ and $Fe_{75}Al_{25}$. Although $Fe_{80}Al_{20}$ conserves the disordered A2 structure and $Fe_{75}Al_{25}$ changes its state of order from DO_3 to B2 and to A2, the temperature variations of H_M(Sch) follow parallel slopes. This is less the case for H_M(Fly): at high temperature, the values of H_M(Fly) tend to the same value, reflecting the fact that the slopes at the origin of the phonon dispersion curves tend to the same values when the temperature is increased.

Surprisingly, the effect of the state of order on H_M seems to be weak.

6. Discussion of results

The main result of the present investigation is the determination of the migration enthalpies in $Fe_{1-x}Al_x$ alloys from the total phonon spectra using Schober's model. This approach yields relatively low values of H_M that decrease with temperature and present a minimum at the Fe_3Al composition.

As similar determinations of H_M have been recently performed by Randl *et al* (1995) on $Fe_{1-x}Si_x$ alloys ($x = 0.2$ and 0.25) at 300 K, the first part of our discussion (section 6.1) will be devoted to a comparison of the results for the two systems. In the second part (section 6.2), we will focus on a more general discussion of the activation enthalpy (H_A) of Fe_3Al, as deduced from diffusion measurements in the A2 and B2 phases, and from ordering kinetics in the DO_3 phase. Taking into consideration the effect of the long-range ordering on the activation enthalpy, we will try to explain the general trend observed experimentally, namely an increase of H_A from the disordered A2 to the ordered B2 phase, followed by an important decrease in the ordered DO_3 phase.

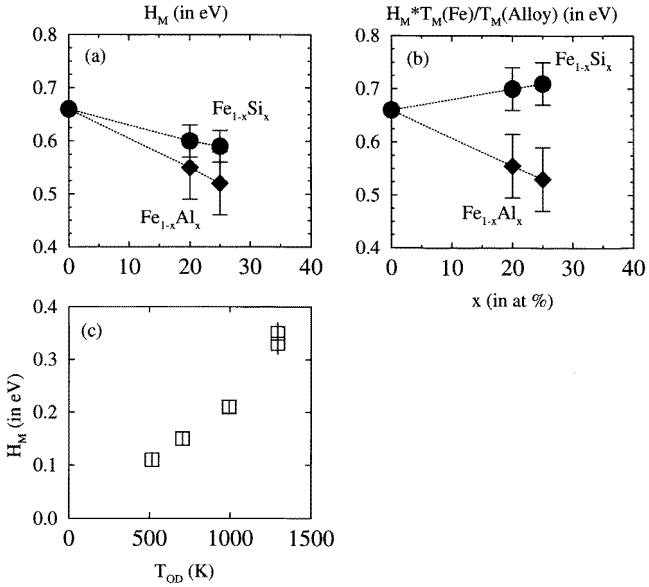

Figure 8. (*a*) Migration enthalpies in the Schober model at 300 K for $Fe_{1-x}Al_x$ (♦) and for $Fe_{1-x}Si_x$ (●) (Randl *et al* 1995). Dotted lines are guides for the eyes. (*b*) Migration enthalpies in the Schober model normalized with the melting temperature ratio T_M(Fe)/T_M(Alloy). (*c*) The dependence of the migration enthalpy on the order–disorder transition temperature in the B2 phase from Monte Carlo simulations using an Ising model (Yaldram *et al* 1995) with pair interactions between first- and second-nearest neighbours and without saddle-point energies.

6.1. Comparison with Fe–Si data

In figure 8(*a*) and table 2 we compare our values of H_M(Sch) with those calculated by Randl *et al* (1995) for $Fe_{1-x}Si_x$ alloys for $x = 0.2$ and 0.25 at 300 K. For each composition H_M is higher in the Fe–Si system than in the Fe–Al system. This difference has for us a real physical meaning. According to the phase diagrams of Kubaschewski (1982), essential differences between the two systems in this concentration range are the melting temperatures and the stability of the ordered structures. For a comparison, we can normalize the H_M(Sch) values with the melting temperatures (T_M), taking as reference the melting temperature of pure Fe. As T_M is higher for Fe_3Al than for Fe_3Si, the difference in H_M is now even greater—about 0.2 eV, as is shown in figure 8(*b*). The different melting temperatures then do not explain the differences between the H_M(Sch)-values of the two systems.

Fe_3Si keeps its long-range-ordered DO_3 structure until its melting point ($T_M = 1500$ K) is reached, indicating that the effective pair interactions that originate the long-range order are much higher than those in Fe_3Al which has lower critical temperatures: the DO_3–B2 order–order transition temperature is 825 K and the B2–A2 order–disorder transition temperature (T_{OD}) is 1040 K. This important difference between the transition temperatures of Fe_3Si and Fe_3Al can cause the difference in the migration enthalpies, as shown in a previous Monte Carlo simulation of ordering kinetics in B2 intermetallic compounds: Yaldram *et al* (1995) have investigated the effect of the relative pair interaction energies (or of the value of T_{OD}) on the amplitude of the migration barrier. The results of this simulation without saddle-point energies (figure 8(*c*)) show that, when T_{OD} increases from 800 to 1500 K, the contribution to the migration barrier due to relative pair interaction energies increases

by about 0.2 eV, a value which is in very good agreement with the difference between H_M in the two systems. Similar Monte Carlo simulations in progress for the DO_3 phase show the same trend.

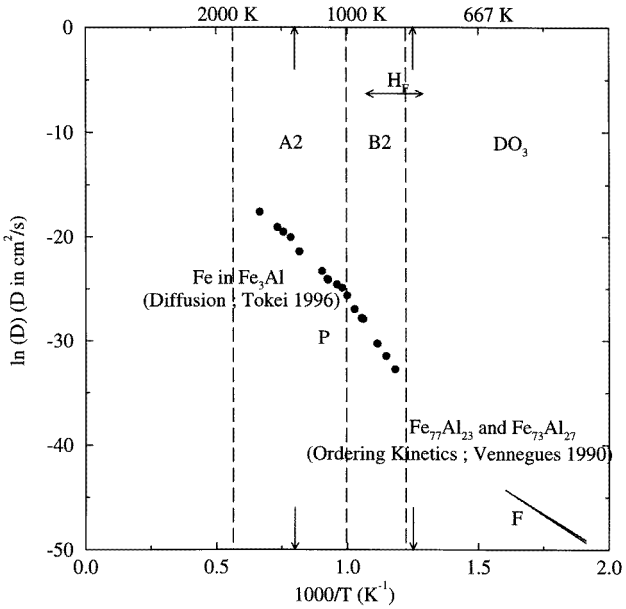

Figure 9. Arrhenius plots of the diffusivities in the Fe–Al system, as described in the text. The dashed vertical lines correspond to A2–B2 and B2–DO_3 transitions. P and F refer respectively to the paramagnetic and ferromagnetic states. The arrows correspond to temperatures where the phonon dispersion curves have been measured.

6.2. The activation enthalpy in Fe_3Al: a comparison between diffusion and ordering kinetics data

In figure 9 we represent on a single plot the recent data obtained via ^{59}Fe self-diffusion through the A2–B2 disorder–order transition of Fe_3Al by Tökei *et al* (1996) and those deduced from ordering kinetics for two Al compositions around Fe_3Al by Vennéguès *et al* (1990) in the DO_3 phase. For these data, the relaxation times τ determined in the ordering kinetics experiments have been changed into diffusivities D using the relation $D = d^2/6\tau$ where d is the nearest-neighbour distance $a\sqrt{3/2}$. The phase stability limits of the ordered structures for the Fe_3Al composition, together with the temperature range of the measurements of the formation enthalpy (H_F) by Schaefer *et al* (1990) are also represented. From figure 9 a curved Arrhenius plot is discernible, i.e. a progressive increase of the activation enthalpy from 1.4 ± 0.2 eV in the low-temperature range (ordering data, DO_3 structure) to an apparent increase in the B2 phase, followed by a decrease of H_A (2.12 eV) in the disordered phase. The same general trend had already been observed by Hasaka *et al* (1993) in diffusion experiments on boron in Fe–26 at.% Al over a T-range covering the A2, B2 and DO_3 structures.

The downward curvature of the Arrhenius plot in the B2 phase was assigned by Tökei *et al* to the contribution of the long-range ordering, according to a mean-field model

developed by Girifalco (1964). This model yields for the activation enthalpy in an ordered B2 compound the following dependence:

$$H_A^O = H_A^D(1 + c^{te}\eta^2(T)) \tag{10}$$

where H_A^O and H_A^D are respectively the activation enthalpies in the ordered and the disordered phase, η is the long-range-order parameter and the constant is related to pair interaction energies. This formalism is currently used by experimentalists to describe the effect of magnetic or chemical order on the activation enthalpy of the diffusion in ferromagnetic or long-range-ordered B2 phases. See for example recent data on Fe and Co self-diffusion in the equiatomic FeCo alloys given by Iijima and Lee (1995). However, the formulation of the activation enthalpy in ordered phases according to relation (10) has to be cautiously considered. Further developments of the theory by Schoijet and Girifalco (1968) show that higher orders in η and terms taking into account the short-range order appear in the formulation of H_F and H_M when approximations of order higher than that of the Bragg–Williams theory are considered. In general, the activation enthalpies in the ordered phase (H_A^O) are deduced from experimental fits of the Arrhenius plot through the relations

$$D = D_0 \exp(-H_A^D)(1 + c^{te}\eta^2)/k_B T = D_0 \exp(-H_A^O/k_B T) \tag{11}$$

in a temperature range close to the order–disorder transition where $\eta(T)$ decreases very rapidly with temperature. For these reasons, the values of H_A^O, obtained for B2 Fe_3Al by Tökei *et al* (1996) and for B2 FeCo by Iijima and Lee (1995) through this very crude model are not very reliable, being not directly measured. This remark is all the more valid for Fe_3Al as this compound does not conserve the B2 structure down to 0 K, but undergoes a B2–DO_3 transition at 825 K. For the above-evoked reasons we will not comment on the various measurements of H_F, H_M and H_A for the B2 range of Fe_3Al. We will restrict our discussion to the DO_3 region and to the disordered solid solution.

For DO_3 Fe_3Al, there are no diffusion measurements available over the stability range of the DO_3 phase, as the diffusivity is too low. We have data on the ordering kinetics for Fe_3Al that yield a low activation enthalpy (H_A^{OK}) of 1.4 ± 0.2 eV (Vennéguès *et al* 1990). This value has to be considered as an average value of the mobility of the two kinds of atom. Combining our present results on the migration enthalpy in the DO_3 phase with the determination of the vacancy formation enthalpy (H_F) over the 773–903 K T-range (Schaefer *et al* 1990), we are able to compare the sum $H_A = H_F + H_M$ to the separately determined H_A^{OK}-value. One gets at 300 K

$$H_A = (0.52 \pm 0.06) + (1.18 \pm 0.04) = 1.70 \pm 0.10 \text{ eV}. \tag{12}$$

Let us note that H_F and H_M are also average quantities. This value of H_A falls within the error bar of the value of H_A^{OK} deduced from ordering kinetics. For the H_M(Fly) values, the agreement is still better. Thus, as long as all of the experimental quantities H_A^{OK}, H_M and H_F represent average quantities and they have been determined for the same structure over equivalent T-ranges, the relationship $H_A = H_F + H_M$ is verified, thus giving good support to our determination of H_M through the above-described phonon method.

Coming back to the data on the disordered phase, our value of H_M (0.39 eV) compared to the value of H_A^{Fe} (2.12 eV from Tökei *et al* 1996) would give a formation enthalpy for the disordered phase of 1.73 eV. This value is close to the value measured for pure iron (1.8 eV from Schultz 1991). It is also the value obtained by using the relationship between H_F and the melting temperature T_M ($H_F/T_M = 1 \times 10^{-3}$ eV K^{-1}) which is generally fulfilled for bcc metals, yielding for Fe_3Al ($T_M = 1775$ K) $H_F = 1.8$ eV. Such an increase of the formation enthalpy of the vacancies from the ordered structures to the disordered ones

would be also responsible for the downward curvature of the Arrhenius plot, together with the contribution of the atomic ordering effect.

7. Conclusion

The phonon dispersion curves have been measured for three $Fe_{1-x}Al_x$ compounds and alloys at three temperatures. From a Born–von Kàrmàn fit of the measured points we have been able to calculate the phonon densities of states necessary to calculate the migration enthalpy using a model proposed by Schober.

A good estimation of the migration enthalpy in iron-rich FeAl as a function of concentration and temperature and for various states of order is thus obtained. One observes a clear minimum of H_M at the DO_3 stoichiometry. Somewhat surprisingly the change of the LRO with increasing temperature has a minor effect on H_M. Rather, H_M decreases with increasing temperature as a pure consequence of increasing anharmonicity. Shifts with temperature of the acoustic phonon branch $T_1[\xi\xi 0]$ or $\Sigma_3^{(1)}$ are indicative of that. Such a temperature-dependent H_M has also been observed for pure bcc metals (Schober *et al* 1992, Güthoff *et al* 1994).

A comparison with the H_M-values for DO_3 Fe–Si compounds obtained through the same approach shows values of H_M clearly higher in Fe–Si than in Fe–Al for a given concentration. This difference is assigned to the contribution of the effective pair interaction energies to H_M that are higher in Fe–Si than in Fe–Al, in very good agreement with previous and current Monte Carlo calculations.

At low temperature, for the DO_3 structure, the three separate determinations of H_M, H_F and H_A, which are average quantities, are consistent, i.e. they obey the relation: $H_A = H_F + H_M$ within the error bars of their determinations. At high temperature in the solid-solution phase, where H_F has not been measured, the difference $H_A - H_M$ yields a value of H_F consistent with the usual relationship $H_F/T_M = 1 \times 10^{-3}$ eV K^{-1}, but clearly higher than in the ordered phase. Such an increase would find a reasonable explanation in the disappearance of the structural vacancies when passing from the ordered state to the disordered one.

Acknowledgments

We would like to thank Dr W Reichardt who provided us with a program to fit the phonon dispersion curves. This program was also very helpful for finding adequate Brillouin zones where the different phonon branches had to be measured at their structure factor maximum. We are also indebted to Professor J M Sanchez for giving us the LRO parameter values as functions of temperature for $Fe_{75}Al_{25}$.

References

Afyouni M 1989 *PhD Dissertation* Louis Pasteur University, Strasbourg
Afyouni M, Pierron-Bohnes V and Cadeville M C 1989 *Acta Metall.* **9** 2339
Ait Salem M, Springer T, Heidemann A and Alefeld B 1979 *Phil. Mag.* A **39** 797
Balanzat E and Hillairet J 1981 *J. Phys. F: Met. Phys.* **11** 1977
Cadeville M C, Pierron-Bohnes V and Sanchez J M 1992 *J. Phys.: Condens. Matter* **4** 9053
Feldwisch R, Sepiol B and Vogl G 1995 *Acta Metall. Mater.* **43** 2033
Flynn C P 1968 *Phys. Rev.* **171** 682
Girifalco L A 1964 *J. Phys. Chem. Solids* **24** 323
Göltz G, Heidemann A, Mehrer H, Seeger A and Wolf D 1980 *Phil. Mag.* A **41** 723

Güthoff F, Hennion B, Herzig C, Petry W, Schober H R and Trampenau J 1994 *J. Phys.: Condens. Matter* **6** 6211
Hasaka M, Morimura T and Kondo S 1993 *Scr. Metall. Mater.* **29** 967
Herzig C 1983 *Diffusion in Metals and Alloys, DIMETA-82* ed F J Kedves and D L Becke (Switzerland: Trans. Tech.) p 23
Iijima Y and Lee C G 1995 *Acta Metall. Mater.* **43** 1183
Kentzinger E 1996 *PhD Dissertation* Louis Pasteur University, Strasbourg (available on request)
Köster W and Gödecke T 1980 *Z. Metallk.* **71** 765
Kubaschewski O 1982 *Iron Binary Phase Diagrams* (Berlin: Springer) pp 136–9
Larikov L N, Geichenko V V and Fal'chenko V M 1981 *Diffusion Processes in Ordered Alloys* (New Dehli: Oxionian) pp 111–7
Leamy H J, Gibson E D and Kayser F X 1967 *Acta Metall.* **15** 1827
Lehman G W, Wolfram T and De Wames R E 1962 *Phys. Rev.* B **15** 1593
Lubbehusen M and Mehrer H 1990 *Acta Metall. Mater.* **38** 283
Peterson N L 1978 *J. Nucl. Mater.* **69-70** 3
Petry W 1995 *J. Physique Coll.* IV (*J. Physique Suppl.* III **5**) C2 15, 28
Petry W, Heiming A, Herzig C and Trampenau J 1991 *Defect Diffusion Forum* **75** 211
Pierron-Bohnes V, Lefebvre S, Bessiere M and Finel A 1990 *Acta Metall. Mater.* **38** 2701
Pierron-Bohnes V, Leroux C, Ambroise J P, Mennelle A and Bastie P 1989 *Phys. Status Solidi* a **116** 529
Raghunathan V S and Sharma B D 1981 *Phil. Mag.* A **43** 427
Randl O G 1994 *PhD dissertation* University of Vienna
Randl O G, Vogl G, Petry W, Hennion B, Sepiol B and Nembach K 1995 *J. Phys.: Condens. Matter* **7** 5983
Robertson I M 1991 *J. Phys.: Condens. Mater* **3** 8181
Sanchez J M 1995 University of Texas at Austin, private communication
Schaefer H E, Würschum R, Sob M, Zak T, Yu W Z, Eckert W and Banhart F 1990 *Phys. Rev.* B **41** 11 869
Schober H R, Petry W and Trampenau J 1992 *J. Phys.: Condens. Matter* **4** 9321
Schoijet M and Girifalco L A 1968 *J. Phys. Chem. Solids* **29** 911
Schultz H 1991 *Landolt–Börnstein New Series* Group III, vol 25, ed H Ullmaier (Berlin: Springer)
Sepiol B and Vogl G 1993 *Phys. Rev. Lett.* **71** 731
Tökei Z, Bernardini J, Gas P and Beke D L 1996 *Acta Metall. Mater.* submitted
Van Dijk C 1970 *Phys. Lett.* **32A** 255
Vennéguès P, Cadeville M C, Pierron-Bohnes V and Afyouni M 1990 *Acta Metall. Mater.* **38** 2199
Vogl G, Petry W, Flottmann T and Heiming A 1989 *Phys. Rev.* B **39** 5025
Yaldram K, Pierron-Bohnes V, Cadeville M C and Khan M A 1995 *J. Mater. Res.* **10** 1